Influence of the Lower-Hybrid Drift Instability on Magnetic Reconnection in Asymmetric Configurations

V. Roytershteyn,[1] W. Daughton,[2] H. Karimabadi,[1] and F. S. Mozer[3]
[1]University of California, San Diego, La Jolla, California 92093, USA
[2]Los Alamos National Laboratory, Los Alamos, New Mexico 87545, USA
[3]Space Sciences Laboratory, University of California, Berkeley, Berkeley, California, USA
(Received 13 September 2011; published 1 May 2012)

Using fully kinetic 3D simulations of magnetic reconnection in asymmetric antiparallel configurations, we demonstrate that an electromagnetic lower-hybrid drift instability (LHDI) localized near the X line can substantially modify the reconnection mechanism in the regimes with large asymmetry, a moderate ratio of electron to ion temperature, and low plasma β. However, the mode saturates at a small amplitude in the regimes typical of Earth's magnetopause. In these cases, LHDI-driven turbulence is predominantly localized along the separatrices on the low-β side of the current sheet, in agreement with spacecraft observations.

DOI: 10.1103/PhysRevLett.108.185001 PACS numbers: 52.35.Vd, 52.65.−y, 94.30.cq

Magnetic reconnection is a ubiquitous phenomenon frequently associated with the fast release of magnetic energy in many systems in nature. One of the long-standing problems in magnetic reconnection research has been the understanding of the reconnection mechanism in collisionless plasmas. Specifically, microscopic turbulence originating from current-driven instabilities has long been considered a possible source of anomalous resistivity (e.g., [1]), with the lower-hybrid drift instability (LHDI) attracting particular attention (e.g., [2]). In a neutral sheet, LHDI can be excited in a relatively broad range of wave numbers $(m_e/m_i)^{1/4} \lesssim k\rho_e \lesssim 1$, where m_s and ρ_s refer to the mass and thermal gyroradius of species s [3]. While the short-wavelength LHDI modes are confined to the low-β periphery of the current sheet, the long-wavelength modes may directly influence the reconnection process since they penetrate the region around the X line, provided the current sheet width is below ρ_i. Electromagnetic fluctuations in the lower-hybrid range have been observed in the vicinity of reconnection sites in both space (e.g., [4–6]) and laboratory plasmas (e.g., [7]). Recent simulations suggested that the long-wavelength modes may expedite the onset of reconnection in a Harris sheet (e.g., [8]) and can be unstable in asymmetric current layers [9]. However, a systematic understanding of the regimes where LHDI plays a significant role in controlling the reconnection process remains elusive.

In this Letter we address the influence of LHDI on reconnection in asymmetric antiparallel geometry, which is relevant, for example, to Earth's magnetopause and some laboratory experiments, such as the Magnetic Reconnection eXperiment [10]. This configuration is characterized by large density gradients across reconnection layers that are favorable for the excitation of LHDI. In contrast to many previous investigations, we focus on long-time dynamics of self-consistently generated current sheets. The results obtained in model 1D equilibria do not directly apply to this problem, since the structure of such layers is determined self-consistently by plasma parameters in the inflow and downflow regions and is not well approximated by existing models. In addition, convective flow through the reconnection region, which is absent from model equilibria, introduces stringent constraints on the growth rate of relevant instabilities. Assuming that the instability of interest is localized on spatial scales comparable to the size of the current sheet, the time scale associated with electron flow through the region of mode localization can be of the order of several $\omega_{\mathrm{LH}}^{-1} = (\omega_{ci}\omega_{ce})^{-1/2}$, where $\omega_{cs} = (|q_s|B)/(m_s c)$, B is the upstream magnetic field, q_s is the charge of species s, and c is the speed of light. Only instabilities that grow faster than the convective time can modify the reconnection dynamics near the X line.

Linear theory and two-dimensional simulations suggest that a correct numerical description of LHDI requires highly expensive simulations with large values of $m_i/m_e \gtrsim 400$ [3]. In order to address these challenges, we utilized a high-performance particle-in-cell code VPIC [11] to perform petascale simulations. The initial magnetic field is of the form $\boldsymbol{B} = \frac{1}{2}[(B_0 + B_1) - (B_0 - B_1)\tanh(z/\delta)]\boldsymbol{e}_x$. The simulations are initialized with two particle populations, a Harris-like component with distribution function $f_s = n_{cc}\cosh^{-2}(z/\delta)\exp[-m_s(\boldsymbol{v} - U_s\boldsymbol{e}_y)^2/(2T_s^0)]$, and an asymmetric Maxwellian component with density $n(z) = (n_0 + n_1)/2 - (n_0 - n_1)\tanh(z/\delta)/2$ and temperature T_s^0. Throughout the text, index "0" denotes values taken on the high-β side of the current sheet at $t = 0$, while the local time-evolving quantities do not have an index. The initial configuration is parameterized by the value of plasma $\beta_0 = 8\pi n_0(T_e^0 + T_i^0)/B_0^2$ and the ratio n_1/n_0 between densities on the low-β and the high-β sides. Typical values considered are $\beta_0 = (0.5 - 2)$ and $n_1/n_0 = (0.1 - 0.2)$. The initial configuration does not

correspond to an exact Vlasov equilibrium, but is in force balance and allows reconnection to develop after a few Alfvén times. While the factors controlling the structure of developed reconnection layers are not completely understood at the present time, existing computer simulations suggest that in collisionless plasma this structure is to a large degree determined by the conditions in the inflow and (to a lesser degree) in the outflow regions. In our simulations the inflow parameters are effectively prescribed by the boundary conditions. Therefore we expect that the details of the initial configuration and the associated transient evolution do not play a key role in determining the structure of the resulting reconnection layers. It is in this sense that we call these layers self-consistent. The inflow boundaries are driven by applying electric field $E_y = E_y^0[1 - e^{-t/\tau}]$, where $E_y^0 = 0.08 B_0 V_A^0$, $\tau = 20(\omega_{ci}^0)^{-1}$, and $V_A^0 = d_i^0 \omega_{ci}^0$. In order to study the evolution of the system over a long time scale, the simulations employed open downstream boundary conditions that allow plasma and electromagnetic flux to leave the simulation domain [12]. Overall, seven simulations with various initial conditions were performed as part of this study. Here we focus on three cases with $\beta_0 = 0.5$, $n_1/n_0 = 0.1$, $T_i^0/T_e^0 = 3$, 1, 0.3, and $m_i/m_e = 400$. Representative numerical parameters for the $T_i^0/T_e^0 = 1$ case are $\omega_{pe}^0/\omega_{ce}^0 = 1.5$, spatial domain $(15 \times 15 \times 15) d_i^0$ with 1152^3 cells, and time step $\Delta t \omega_{ce}^0 \approx 0.1$. The plasma at $t = 0$ was represented by 0.7×10^{12} computational particles. Here $d_s^0 = c/\omega_{ps}$, $\omega_{ps} = (4\pi n_0 q_s^2/m_s)^{1/2}$.

Figure 1 demonstrates spatial localization of the electromagnetic fluctuations in a simulation with $T_i^0/T_e^0 = 3$. The two panels show fluctuation power $\langle |F|^2 \rangle = \sum_{\omega,k} |F(\omega, k_y)|^2$, with $F = \tilde{E}_y$ (top panel) and $F = \tilde{B}_x$ (bottom panel). Here the sum is over $0 < \omega < 3\omega_{\rm LH}$ and $k_y \rho_e < 2$. The spectra are computed over an interval $t\omega_{ci}^0 = (39 - 44)$. It is immediately apparent that the fluctuations along the separatrices produce predominantly perturbations of the electric field, while the perturbations of the magnetic field are localized around the X line. In Fig. 1, the power of $\tilde{B}_x$ is normalized to the magnetic field immediately upstream from the layer on the low-β side B_e^2, while that of $\tilde{E}_y$ is normalized to E_A^2, where $E_A = (\omega_{\rm LH}/\omega_{pe}) B_e$ is a typical amplitude that can be expected for a mode of frequency $\omega_{\rm LH}$ localized on spatial scales of the order of d_e. The (ω, k_y) spectra of E_y and B_x fluctuations are shown in Fig. 2 for locations close to the X line and at the separatrices on the low and high sides of the current sheet, as marked by large dots in the Fig. 1(a). Near the X line the dominant perturbation has a characteristic wavelength $k_y(\rho_e \rho_i)^{1/2} \sim 1$ and produces strong perturbations of the magnetic field, in agreement with the expectations based on linear theory of Harris equilibrium [3]. In contrast, the fluctuations along the separatrices have a broader spectrum, with stronger perturbations of E_y. The frequency corresponding to the center of the spectrum follows a local dispersion relation for the LHDI [13]. The separatrices on the high-β side are considerably more stable and fluctuations tend to have relatively higher values of $\tilde{B}_x/\tilde{E}_y$. Both of these trends are consistent with linear theory since sharp density gradients and relatively low values of β are conducive to the development of LHDI.

The influence of the long-wavelength LHDI mode on the structure of the reconnection layer in the most unstable case with $T_i^0/T_e^0 = 0.3$ is documented by Figs. 3 and 4. In our simulations a large-scale 2D symmetry is imposed by the choice of initial and boundary conditions. Consequently, considering y-averaged quantities in 3D simulations enables a relatively simple interpretation of the effects introduced by fluctuations. Panels (a), (b) and (c) in Fig. 3 compare the current density between 2D and

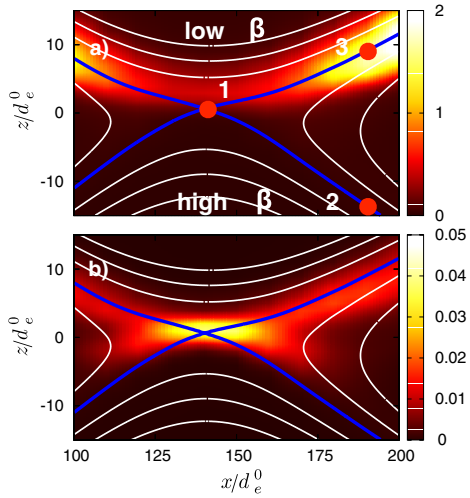

FIG. 1 (color online). Power of $\tilde{E}_y$ (top) and $\tilde{B}_x$ (bottom) fluctuations in the range $|\omega| < 3\omega_{\rm LH}$ and $|k_y \rho_e| < 2$. The solid lines represent the field lines of the y-averaged in-plane magnetic field, with the thick lines marking the separatrix.

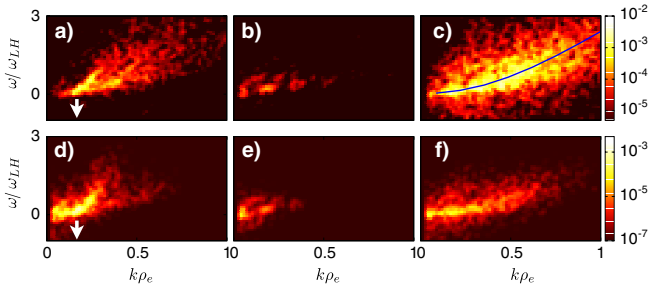

FIG. 2 (color online). Panels (a), (b), and (c): spectrum of $\tilde{E}_y$ fluctuations at positions marked 1, 2, and 3, respectively, in Fig. 1. Panels (d), (e), and (f): the same for $\tilde{B}_x$. The solid line in panel (c) corresponds to the local dispersion relation for LHDI [13]. The arrow in panels (a) and (d) marks $k_y = (\rho_e \rho_i)^{-1/2}$. The values of $\omega_{\rm LH}$ and ρ_s are computed with the shoulder value of the magnetic field and temperatures at the center of the layer.

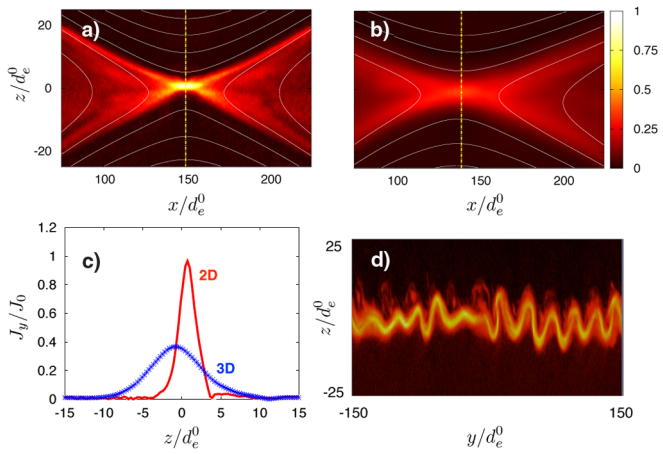

FIG. 3 (color online). Panels (a) and (b) show current density j_y in 2D and 3D simulations, respectively, with $T_i^0/T_e^0 = 0.3$ at $t\omega_{ci}^0 = 42$. Here j_y is normalized to its peak value in the 2D case; (c) profiles of j_y across the layer at x positions marked by dashed lines in panels (a) and (b); Panel (d) shows a profile of j_y in a y-z plane at $x/d_e^0 = 140$ in the 3D simulation.

3D simulations, respectively, and demonstrate that on average the current layer is more than a factor of 2 broader and longer in the 3D simulation. Panel (d) demonstrates the large-amplitude kinking of the layer induced by the development of the long-wavelength instability.

Figure 4 further illustrates properties of the fluctuations both in the reconnection current layer (left column) and at the low-β separatrix (right column). In the reconnection layer, the peak amplitude of the magnetic fluctuations coincides with the X line, while E_y fluctuations are peaked upstream from the X line on the low-β side. At x locations outside of the current sheet, the $\tilde{E}_y$ fluctuations are peaked right on the separatrix and the ratio $\langle|\tilde{E}_y|^2\rangle/\langle|\tilde{B}_x|^2\rangle$ is substantially higher compared to the vicinity of the X line. The modifications in the structure of current layers induced by LHDI fluctuations are associated with changes in the reconnection mechanism. To quantify this, we compute the y average of the electron momentum balance equation $m_e n_e d\boldsymbol{V}_e/dt = -en_e\boldsymbol{E} - \nabla\cdot\boldsymbol{P}_e - en_e(\boldsymbol{V}_e/c)\times\boldsymbol{B}$ and split nonlinear terms into the contribution from average and fluctuating parts. For example, $\langle AB\rangle = \langle\widetilde{AB}\rangle + \langle A\rangle\langle B\rangle$, where $\langle\cdots\rangle$ refers to the average. As is apparent from Fig. 4, the $\langle n_e\widetilde{E_y}\rangle$ term, which represents direct momentum exchange between ions and electrons induced by quasineutral fluctuations, peaks away from the X line, but is still responsible for about 30% of the nonideal field at the X line. The $\langle n_e(\widetilde{\boldsymbol{v}_e\times\boldsymbol{B}})_y\rangle$ term contributes another 30% of $\langle nE_y\rangle$. The remainder of the electric field is supported by the average divergence of electron-stress tensor $(\nabla\cdot\boldsymbol{P}_e)_y$, which is the dominant term in 2D geometry. Note that the $\langle n_e(\widetilde{\boldsymbol{v}_e\times\boldsymbol{B}})_y\rangle$ term peaks at the X line and near the location of the maximum of

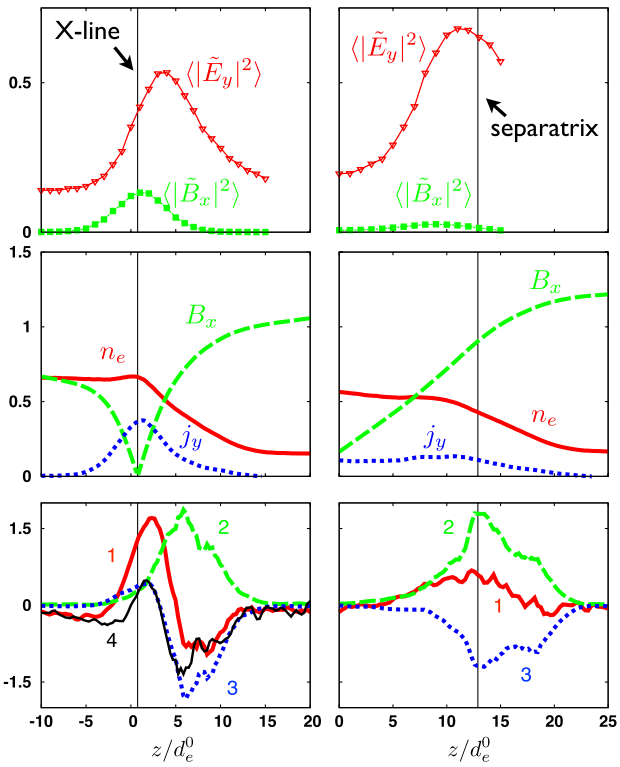

FIG. 4 (color online). Spatial profiles of various quantities in 3D simulation with $T_i^0/T_e^0 = 0.3$ across the reconnection layer (left column, $x/d_e^0 = 140$) and across the separatrix on the low-β side (right column, $x/d_e^0 = 200$). Top row: profiles of fluctuation amplitude. Middle row: profiles of average density, magnetic field, and current. Bottom row: contribution of fluctuations to the average force balance (1) : nonideal term $(\langle\boldsymbol{E}\rangle + \langle\boldsymbol{V}/c\rangle\times\langle\boldsymbol{B}\rangle)_y$; (2): $\langle\widetilde{nE}_y\rangle$; (3): $\langle(n\widetilde{\boldsymbol{V}\times\boldsymbol{B}})_y\rangle$; (4): $\langle(\nabla\cdot\boldsymbol{P})_y\rangle$. All terms are normalized to local $\langle nE\rangle$.

the $\langle n_e\widetilde{E_y}\rangle$ term. Effectively, it exchanges electron momentum between the two regions, thus facilitating momentum exchange between electrons and ions. Finally, even though $\langle n_e\widetilde{E_y}\rangle$ is substantial near the low-β separatrix, LHDI perturbations produced relatively small contributions to the parallel force balance at these locations, i.e., $\langle n_e\widetilde{E_\parallel}\rangle \ll \langle n_e\widetilde{E_y}\rangle$.

In summary, our results demonstrate that under some conditions LHDI may directly influence the reconnection mechanism in the vicinity of the X line. Specifically, in a simulation with $T_i^0/T_e^0 = 0.3$, $\beta_0 = 0.5$ and $n_0/n_1 = 10$, the sum of fluctuation-induced terms accounted for approximately 60% of the average electric field close to the X line with the $\langle\widetilde{nE_y}\rangle \approx 0.3\langle nE_y\rangle$. At the same time, these terms contributed less than 30% of the total field in simulation with $T_i^0/T_e^0 = 3$, with $\langle\widetilde{nE_y}\rangle < 0.05\langle nE_y\rangle$. The saturation amplitude of the fluctuations near the X line decreased almost linearly with T_i^0/T_e^0 from $\langle|\tilde{B}_x|^2\rangle \approx 0.13B_e^2$ in the simulation with $T_i^0/T_e^0 = 0.3$ to $\langle|\tilde{B}_x|^2\rangle \approx 0.04B_e^2$ in the simulation with $T_i^0/T_e^0 = 3$. While the

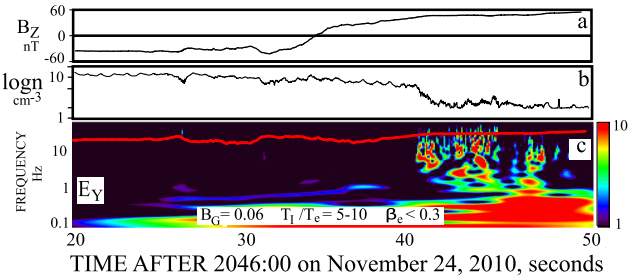

FIG. 5 (color online). A subsolar magnetopause crossing by the THEMIS satellite. Panel (a) shows the reconnection magnetic field, which changed from the negative value in the magnetosheath to the positive value in the magnetosphere. Panel (b) is the plasma density. Panel (c) shows the spectrum of E_y fluctuations, which are localized near the region of large density gradients.

exact numerical values of various thresholds likely depend on the numerical parameters employed in a particular simulation (e.g., m_i/m_e or ω_{pe}/ω_{ce}) and may depend on the boundary conditions employed in a particular simulation (which may influence the structure of the current sheet), we expect the *trends* established in this work to hold. Therefore, we expect that LHDI has the strongest influence on the reconnection process in regimes with large asymmetry, low values of $T_i/T_e < 1$, and low β on both sides of the current sheet. The latter requirement, which emerged from our simulations, is consistent with the properties of linear eigenfunction for a long-wavelength LHDI mode that tunnels through the high-β vicinity of the X line [3]. We also note that the long-wavelength LHDI does not reach substantial amplitude in simulations in a symmetric configuration with comparable values of β and T_i/T_e (except during the decay of the initial configuration), indicating the destabilizing influence of the density gradient across the reconnection layer. Given the above requirements, we conclude that this instability is unlikely to be important for reconnection at the magnetopause, where typically $T_i > T_e$ and $\beta \gtrsim 1$ on the magnetosheath side of the current sheet. On the other hand, it may play a role in other systems. For example, the Magnetic Reconnection eXperiment operates at low values of β and is characterized by smaller T_i/T_e compared to the magnetosphere.

In contrast to the long-wavelength LHDI, the short-wavelength modes excited along the separatrices should persist under conditions typical of the magnetopause. Several recent results indicate that the separatrices may play an important role in controlling the reconnection process and energy release associated with reconnection (e.g., [14,15]). Since short-wavelength LHDI competes with these processes, it may indirectly affect the reconnection process by modifying the structure of the separatrix current layer. For example, we have observed a roughly twofold increase in the average thickness of the separatrix current layer in the 3D simulations discussed in this Letter, which should decrease the growth rate of tearing instabilities developing along the separatrix [14].

The conclusions reached here with regards to the properties of LHDI at Earth's magnetopause are generally consistent with previous investigations of the role of LHDI (e.g., [5]) and with a more recent survey of subsolar magnetopause crossings by the THEMIS satellite [16]. An example of such a crossing is shown in Fig. 5. In agreement with our expectations, the electric field fluctuations are predominantly localized in the vicinity of the low-β separatrix in the frequency range $\omega \lesssim \omega_{\mathrm{LH}}$ and are relatively weak within the current layer. At the same time, the estimates of $\langle \widetilde{nE_y} \rangle$ obtained from observations are much smaller than $\langle nE_y \rangle$ even near the separatrices, which is likely due to the differences in plasma parameters (β, T_i/T_e, degree of asymmetry) between the simulations and the observations. A detailed comparison of selected events with matching simulations is under way.

The authors acknowledge support from NSF Grants No. ATM0802380 and No. OCI 0904734, NASA Heliophysics Theory Program, and the LDRD program at Los Alamos. This research used resources of the National Center for Computational Sciences at Oak Ridge National Laboratory, which is supported by DOE under Contract No. DE-AC05-00OR22725. Additional simulations were supported by an allocation of advanced computing resources provided by the NSF at the National Institute for Computational Sciences and by NASA.

[1] E. Priest and T. Forbes, *Magnetic Reconnection: MHD Theory and Applications* (Cambridge University Press, Cambridge, England, 2000); K. Papadopoulos, Rev. Geophys. **15**, 113 (1977).
[2] J. D. Huba, N. T. Gladd, and K. Papadopoulos, Geophys. Res. Lett. **4**, 125 (1977).
[3] W. Daughton, Phys. Plasmas **10**, 3103 (2003).
[4] C. Cattell, J. Wygant, F. S. Mozer, T. Okada, K. Tsuruda, S. Kokubun, and T. Yamamoto, J. Geophys. Res. **100**, 11823 (1995).
[5] S. D. Bale, F. S. Mozer, and T. Phan, Geophys. Res. Lett. **29**, 2180 (2002).
[6] M. Zhou *et al.*, J. Geophys. Res.**114**, A02216 (2009).
[7] T. A. Carter, M. Yamada, H. Ji, R. M. Kulsrud, and F. Trintchouk, Phys. Plasmas **9**, 3272 (2002); H. T. Ji, S. Terry, M. Yamada, R. Kulsrud, A. Kuritsyn, and Y. Ren, Phys. Rev. Lett. **92**, 115001 (2004); W. Fox, M. Porkolab, J. Egedal, N. Katz, and A. Le, Phys. Plasmas **17**, 072303 (2010).
[8] R. Horiuchi and T. Sato, Phys. Plasmas **6**, 4565 (1999); K. Fujimoto, *ibid.* **16**, 042103 (2009); **18**, 111206 (2011).
[9] P. L. Pritchett and F. S. Mozer, J. Geophys. Res. **116**, 7 (2011).

[10] M. Yamada, H. Ji, S. Hsu, T. Carter, R. Kulsrud, N. Bretz, F. Jobes, Y. Ono, and F. Perkins, Phys. Plasmas **4**, 1936 (1997).
[11] K. J. Bowers, B. J. Albright, L. Yin, B. Bergen, and T. J. T. Kwan, Phys. Plasmas **15**, 055703 (2008).
[12] W. Daughton, J. Scudder, and H. Karimabadi, Phys. Plasmas **13**, 072101 (2006).
[13] R. C. Davidson, N. T. Gladd, C. S. Wu, and J. D. Huba, Phys. Fluids **20**, 301 (1977).
[14] W. Daughton, V. Roytershteyn, H. Karimabadi, L. Yin, B. J. Albright, B. Bergen, and K. J. Bowers, Nature Phys. **7**, 539 (2011).
[15] J. Egedal, A. Lê , Y. Zhu, W. Daughton, M. Øieroset, T. Phan, R. P. Lin, and J. P. Eastwood, Geophys. Res. Lett. **37**, 5 (2010).
[16] F. Mozer, M. Wilber, and J. F. Drake, Phys. Plasmas **18**, 102902 (2011).